

Automatic Ice Boundary Detection in Radar Echograms based on Charged Particles Concept

Maryam Rahnemoonfar^{1*}, *Member, IEEE*, John Paden², Geoffrey C. Fox³

Accelerated loss of ice from Greenland and Antarctica has been observed in recent decades. Ice thickness is a key factor in making predictions about the future of massive ice reservoirs and can be estimated by calculating the exact location of the ice surface and bottom in radar imagery. Identifying the locations of ice boundaries is typically performed manually which is a very time consuming procedure. Here we propose a novel approach which automatically detects the complex topology of ice surface and bottom boundaries based on charged particle concept. Here we first applied anisotropic diffusion to remove the noise and enhance the image. At the second step, we detected the contours in the image based on Coulomb's electrostatic law and the assumption that each pixel is an electrically charged particle. The final ice surface and bottom are detected based on the projection profile of the contours. The results are evaluated on a large dataset of airborne radar imagery collected during IceBridge mission over Antarctica and show promising results with respect to hand-labeled ground truth and an state-of-the-art algorithm.

Index Terms—*Remote sensing, image analysis, radar*

I. INTRODUCTION

Serious damages have been caused to our environment by global warming. In recent decades, accelerated loss of ice from Greenland and Antarctica has been observed [1]. The melting of polar ice sheets and mountain glaciers has a significant influence on sea level rise and flooding of coastal regions. The Intergovernmental Panel on Climate Change (IPCC) estimates that sea level could increase by 26 – 98cm by the end of this century. The large range in predicted sea-level rise can be partially attributed to an incomplete understanding of bed topography and basal conditions of fast-flowing regions of the ice sheets in Greenland and Antarctica. Therefore precise calculation of ice thickness is very important for sea level and flood monitoring. Moreover the shape of the landscape hidden beneath the thick ice sheets is a key factor in predicting ice flow and their future contribution to sea level rise in response to a changing climate. Therefore, it is important to develop fully automatic techniques for detecting ice surface and subglacial topography hidden beneath the thick ice sheets. To provide important information about ice sheet thickness, the

multichannel coherent radar depth sounder was used during the IceBridge mission [2]. In this work the images are the CReSIS standard output product [3] and by using pulse compression, synthetic aperture radar (SAR) processing, and multi-looking they are formed. The complete processing details are provided in Gogineni et al. [4]. Figure 1 shows a sample radar echogram gathered by the multichannel coherent radar depth sounder where the top line is the boundary of ice and air, ice surface, and the bottom line is the boundary between ice and the subglacial topography, ice bottom. The horizontal axis is the flight path and the vertical axis is the ice depth.

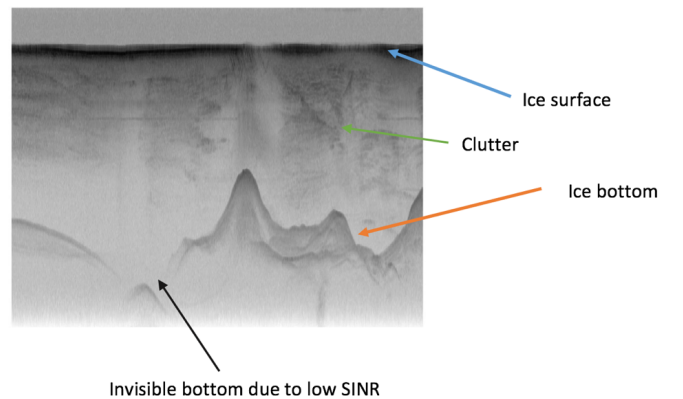


Fig. 1. Ice surface and bottom depicted in radar echograms.

As it can be seen in Figure 1 the ice bottom in radar echogram suffer from low signal to interference and noise ratios (SINR). Low SINR is caused by several factors such as signal attenuation while traveling through ice, radar clutter energy, and thermal noise and occasional electromagnetic interference. Moreover, the ice bottom shape varies from flat to mountainous. Finally, artifacts in the data, such as surface multiples, can lead to false identification of the ice bottom layer. These are all the challenging factors in automatic ice and bottom detection.

In this paper a novel contour detection method is developed to automatically identify the ice surface and bottom layers in a large dataset of radar imagery. In this approach, an electrically charged particle plays a role of a pixel that has electrostatic interaction with other neighboring particles/pixels. The grayscale intensity of the pixel will represent electrical charge of each particle indirectly. After setting some rules to create similar characteristics between electrical charges and image pixels, a novel kernel and contour detection formula is developed based on the interaction between charged particles and their electrical

1. Department of Computing Sciences, Texas A&M University-Corpus Christi, Corpus Christi, TX

2. Center for Remote Sensing of Ice Sheets, University of Kansas, Lawrence, KS

3. School of Informatics and Computing, Indiana University, Bloomington, IN

* Corresponding Author

files. To improve the quality of counter detection, the images were first enhanced by anisotropic diffusion [5] and the final layers were extracted by calculating the local maxima in the projection profile. After this introduction, related works will be reviewed in section 2. The details of the proposed method will be discussed in section 3. Experimental results and evaluation will be discussed in section 4. Finally conclusion is drawn in section 5.

II. RELATED WORKS

For layer finding and ice thickness in radar images the common practice is that human experts mark ice sheet layer and bedrock by hand, which is a very time consuming and tiresome task and may create errors. In recent years, several semi-automated and automated methods have been introduced in the literature [6], [7], [8], [9], [10], [11], [12], [13], [14], [15], [16], [17], [18], [19], [20], [21], [22], [23].

Freeman et al. [9] and Ferro & Bruzzone [8] extracted ice layers from the shallow subsurface radar on NASA's Mars reconnaissance Orbiter (SHARAD). Crandall et al [6] used probabilistic graphical models for detecting ice layer boundary in echogram images from Greenland and Antarctica. The extension of this work was presented in [14] where they used Markov-Chain Monte Carlo to sample from the joint distribution over all possible layers conditioned on an image. A Gibbs sampling instead of dynamic programming based solver was used for performing inference. The problem with using graphical models is that it needs a lot of training samples (around half of the actual dataset) which can be very time-consuming to be labeled manually by a human. In another work, Gifford [11] compared the performance of two methods, edge based and active contour, for automating the task of estimating polar ice and bedrock layers from airborne radar data acquired over Greenland and Antarctica. They showed that their edge-based approach offers faster processing but suffers from lack of continuity and smoothness that active contour provides. Mitchell et al [15] used a level set technique for estimating bedrock and surface layers. However, for each single image the user needs to re-initialize the curve manually and as a result the method is quite slow and was applied only to a small dataset. This problem was fixed in [21], [22] where authors introduced a distance regularization term in the level set approach to maintain the the regularity of level set intrinsically. Therefore, it does not need any manual re-initialization and was automatically applied on a large dataset. However, their technique has a difficulty in detecting the ice bottom when it is faint. Our proposed approach based on electric charged particles address this issue efficiently.

Most of the pioneering methods in contour detection are based on quantifying the presence of a boundary at a given location in the image. The Roberts [24], Sobel, and Prewitt [25] operators detect edges by convolving an image with given operators. Marr and Hildreth [26] use zero crossings of the Laplacian of Gaussian operator. The Canny method [27] uses non-maximum suppression and hysteresis thresholding steps to model sharp discontinuities in a given image. In recent years, new contour detection approaches have been explored

such as methods based on statistical approaches [28] [29], morphological gradients [30], [31], Contour saliency [32], active contours [33] [34] [35] [36], neural networks [37] [38], fuzzy logics [39] [40], rule base [41], gravity [42] [43], supervised learning [44], hierarchal segmentation [45] and sparse code gradient [46]. Although recent methods proved to outperform the old methods, most common implementations still concern the simple pioneering methods.

Our proposed method is inspired by the gravitational method in [42]. The edge detection methodology in [42] is based on theory of universal gravity. Here, we used Coulomb's Law of electrostatic force [47] to extract the image contours. There are some differences between gravitational force and electrostatic force. One major difference lies in the strength of the forces. The gravitational attraction between two electrons is only 8.22×10^{-37} of the electrostatic force of repulsion at the same separation. Another difference is that the gravitational force is concerned with large masses and always attracts, while electrical forces are concerned with small particles and attract when the electrical charges are opposite and repel if the charges are similar. We believe having both attractive and repulsive forces will improve the contour detection performance.

III. METHODOLOGY

Our method consists of three main steps: 1-anisotropic diffusion to remove the noise and enhance the quality of the image while preserving the edges. 2-EIFi method which is our proposed contour detection algorithm based on the theory of electrostatic and 3-projection profile to extract the layers of ice surface and bottom from the output of contour image.

A. Anisotropic Diffusion

Radar imagery suffers from low signal to interference and noise ratios (SINR). It is necessary to remove noise prior to any contour detection algorithm. However most of the enhancing techniques, in addition to removing noise will affect the quality of edges and contours. Here we used anisotropic diffusion technique[5] which remove the noise while preserving the contour's quality.

The anisotropic diffusion equation is defined as[5]:

$$\begin{cases} I_t = \text{div}(c(x, y, t) \nabla I) \\ I_t = c(x, y, t) \Delta I + \nabla c \cdot \nabla I \end{cases} \quad (1)$$

where div is divergence operator, ∇ is the gradient operator and Δ is the Laplacian operator. Assuming $c(x, y, t)$ as a constant, the isotropic heat diffusion equation will be:

$$I_t = c \Delta I \quad (2)$$

This method undergoes smoothing filter within a region as opposed to smoothing across the boundaries by setting the conduction coefficient in the interior to be 1 and 0 at the boundaries of each region. Therefore, the blurring occurs separately in each region with no interaction between regions, which result in sharp boundaries.

B. Contour detection based on electric field

To detect the boundary of ice surface and bottom layers, we developed a novel contour detection technique based on electric field (EIFi).

In the EIFi method, every pixel is assumed to be an electrically charged particle that has electrostatic interaction with other neighboring particles. As it can be seen from Figure 2, charges are either positive or negative and the electrical force between them can be attractive or repulsive. The type of the force, attractive or repulsive, determines the electric field direction, which can be used for contour detection. Since our goal is to find the effect of neighboring pixel on the central pixel, we will use the concept of electrical field instead of electrical force.

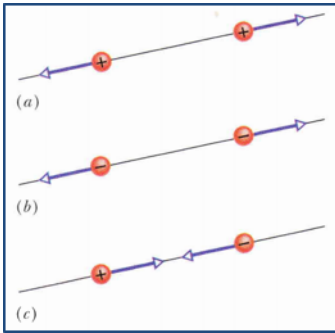


Fig. 2. Repulsive (a, b) and attractive (c) force between electrical charges

To be able to apply the electric field concept on pixel values, first, we need to create similar conditions between charged particles in the real world and the pixels in the image. By comparing the pixel characteristic with particle characteristic, it can be seen that each particle in the real world has two characteristics: firstly, it has a small charge; secondly, the charge can be positive or negative. The pixel values in grey level image vary between 0 and 255 and they are always positive value. Therefore, in the first step, pixel values will be transferred to a range more similar to electrically charged particles according to equation 3:

$$q_i = \frac{2p_i - 2^n + 1}{2^{n+1} - 1} \quad (3)$$

where p_i is the grey level value of pixel i and q_i is the equivalent electrical charge for that pixel. n is the number of bits in the image.

After making pixels resemble electrical charges, it is time to calculate the electrostatic field a pixel exerts on every other pixel around it. Figure 3 shows the interaction of a central pixel with its eight neighbors. As is depicted in Figure 3 for a 3×3 kernel, each pixel has eight neighbors. For four main neighbors (horizontal or vertical), the distance to the central pixel is 1 while it is $\sqrt{2}$ for diagonal neighbors.

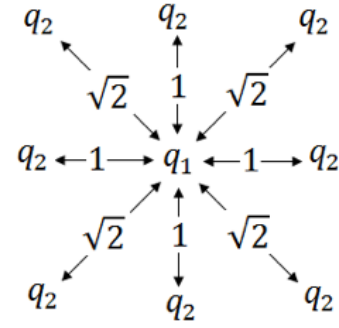


Fig. 3. Distance and relationship between the central pixel and its 8 neighbor pixels

The electric field of a point charge, which is located in the center, can be obtained from Coulomb's law:

$$\vec{E}_1 = \frac{\vec{F}}{q_1} \quad (4)$$

where E_1 is electric field of q_1 particle.

This equation is computed for every neighbor of central pixel. Strong attractive or repulsive electric field is due to a high amount of electric charge of a particle. To detect contours, we used the gradient of pixels rather than the magnitude of each pixel. Therefore, when we are designing our kernel, we use the absolute differential electric field to be able to extract contours. The differential electric field for two neighbor particles is calculated according to equation 5:

$$\Delta E_i(Q_i) = \frac{|Q_i - q_1|}{|r_i|^2} \frac{\vec{r}_i}{|r_i|} \quad (5)$$

where Q_i is the electric charge of the neighbor i and q_1 is the electric charge of central pixel. Finally, the vector sum of all electrical fields is used to calculate the magnitude of signal variation and to detect image contours. For example, for a 3×3 kernel in the image, the equation 5 would be in the following form:

$$\vec{E} = \sum_{s=i-1}^{i+1} \sum_{t=j-1}^{j+1} \frac{|Q(s,t) - Q(i,j)|}{d_{Q(s,t),Q(i,j)}^2} \quad (6)$$

where $Q(s,t)$ is the electric charge of the neighbor pixel and $Q(i,j)$ is the electric charge of central pixel and d is the distance between two pixels.

This equation can be written in the form of a kernel (Figure 4). At any point in the image, the response of kernel is the sum of products of the kernel coefficients and the image pixels encompassed by the filter. Convolution is performed by sliding the kernel over the image, starting at the top left corner, to move the kernel through all the positions where the kernel fits entirely within the boundaries of the image.

$$\begin{bmatrix} \frac{|Q_{i,j} - Q_{i-1,j-1}|}{2} & |Q_{i,j} - Q_{i-1,j}| & \frac{|Q_{i,j} - Q_{i-1,j+1}|}{2} \\ |Q_{i,j} - Q_{i,j-1}| & 0 & |Q_{i,j} - Q_{i,j+1}| \\ \frac{|Q_{i,j} - Q_{i+1,j-1}|}{2} & |Q_{i,j} - Q_{i+1,j}| & \frac{|Q_{i,j} - Q_{i+1,j+1}|}{2} \end{bmatrix}$$

Fig. 4. Electric field 3×3 kernel

Figure 5.b shows the result of applying the EIfi technique on the enhanced SAR image (Figure 5.a) where the top layer is the ice surface and bottom layer is the ice bottom which can be a bedrock or sea surface.

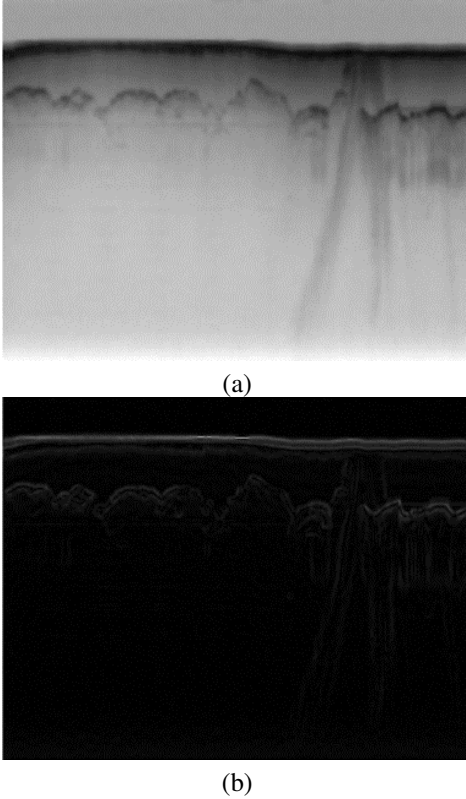


Fig. 5. (a) Enhanced SAR image by Anisotropic diffusion, (b) the result of EIfi technique

C. Projection profile

As it can be seen in Figure 5.b the image contours are highlighted where the ice surface and bottom have brighter values. To extract the exact ice surface and bottom boundaries, we calculated the local horizontal projection profile on every 5 pixels' column. The two local maximum in the projection profile (Figure 6) depicts the location of ice surface and bedrock.

IV. EXPERIMENTAL RESULTS

We applied the proposed approach on the 2009 NASA Operation IceBridge Mission. The images have a resolution of 900 pixels in the horizontal direction, which covers around 50km on the ground, and 700 pixels in the vertical direction,

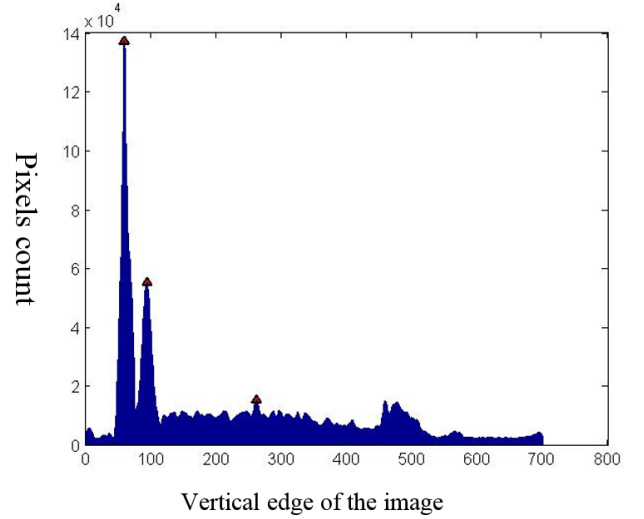


Fig. 6. Horizontal projection profile for local vertical columns

which corresponds to 0 to 4km of ice thickness. We applied our method on total of 323 images and compared the results with the ground-truth. The ground-truth images have been produced by human annotators. Figure 7 shows the results of our approach with respect to the ground-truth. Figure 7.a shows the original image. Figure 7.b shows the result after anisotropic diffusion. As it can be seen in this figure, the image is enhanced while the edges are preserved. This stage is necessary for reducing the noise. At the next step, the EIfi method was applied on the enhanced image. As it can be seen in Figure 7.c EIfi method detects contours in the image. To highlight the ice surface and bottom boundaries, the projection profile of the EIfi result was calculated. Figure Figure 7.d shows all of the points extracted from local maxima of projection profile. Figure 7.e shows the ground-truth results acquired by manually picked layers. The output of our approach shows a satisfactory results compared to the manually picked interfaces.

Figure 8 shows the result of our algorithm with respect to the ground-truth in a diverse dataset which includes images with clutter (all rows), large variability of ice bottom shape from flat (second and last rows) to mountainous (first and third rows), surface multiples (second, forth, and fifth rows), and partially invisible ice bottoms (first and last rows). Left column in Figure 8 shows our results while the right column is the ground-truth (manually picked layers by human).

To evaluate the performance of our approach, we calculated precision (P), recall (R), and F-measure as follow:

$$R = \frac{TP}{TP + FN} \quad (7)$$

$$P = \frac{TP}{TP + FP} \quad (8)$$

where TP is true positive or correct result, FP is false positive or unexpected result, FN is false negative or missing results, and TN is true negative. Precision measures the exactness of a classifier and recall measures the completeness of a classifier.

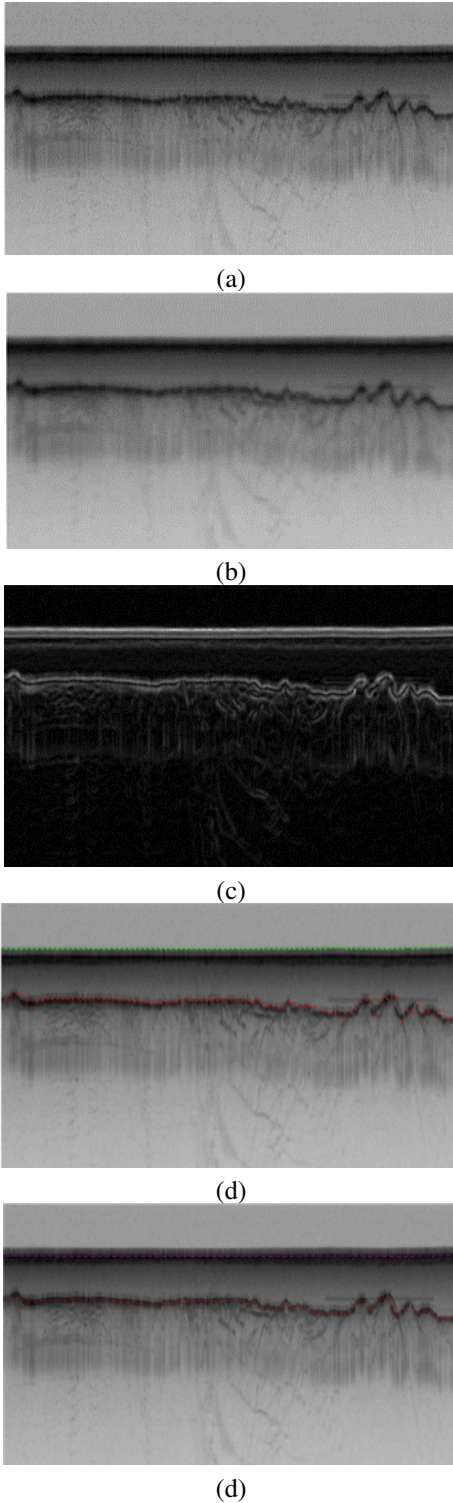


Fig. 7. The result of our approach. a) original image, b) the enhanced image after anisotropic diffusion, c) detected contours with EIfi technique, d) detected ice surface and bottom after projection profile, e) ground-truth

They can be combined to produce a single metric known as *F-measure*, which is the weighted harmonic mean of precision and recall. The F-measure defined as:

$$F = \frac{1}{\alpha \frac{1}{P} + (1 - \alpha) \frac{1}{R}} \quad (9)$$

captures the precision and recall tradeoff. The F-measure is valued between 0 and 1, where larger values are more desirable. Table I shows the average precision, recall, and F-measure on our entire dataset in comparison to the state-of-the-art method [22]. As it can be seen in Table I, we reached a higher accuracy in comparison to the state-of-the-art technique. Part of this is due to the fact that our method is able to detect the faint part of ice bottoms more accurately. By having a closer look at the ice bottom of the image in the first row of Figure 8 we notice that our algorithm is able to detect the ice bottom especially the invisible part more accurately while the technique in [22] have difficulty in detecting the faint part of the ice bottom (see Figure 9).

	Precision	Recall	F-measure
Our results	0.84	0.79	0.81
Rahmemonfar et.al [22]	0.74	0.77	0.75

TABLE I
THE RESULT OF OUR APPROACH ON 2009 NASA OPERATION ICEBRIDGE MISSION

V. CONCLUSION

In this paper we developed a novel approach which automatically detects the complex topology of ice surface and bottom boundaries based on Electric field (EIfi). Here we first applied anisotropic diffusion to enhance the image while preserving the edges. At the second step, the contours were detected based on Coulomb's electrostatic law and the assumption that each pixel is an electrically charged particle. The final ice surface and bottom were detected based on the projection profile of the contours. The results were evaluated on a large dataset of airborne radar imagery collected during IceBridge mission over Antarctica and we reached high accuracy of 81% with respect to hand-labeled ground truth. Our proposed technique could detect the invisible part of ice bottom more accurate than the state-of-the-art technique.

ACKNOWLEDGMENT

This project is partially supported by NSF CIF21 DIBBS 1443054 and Texas Comprehensive Research Funding.

REFERENCES

- [1] A. Shepherd, E. R. Ivins, A. Geruo, V. R. Barletta, M. J. Bentley, S. Bettadpur, K. H. Briggs, D. H. Bromwich, R. Forsberg, N. Galin *et al.*, "A reconciled estimate of ice-sheet mass balance," *Science*, vol. 338, no. 6111, pp. 1183–1189, 2012.
- [2] C. Allen, L. Shi, R. Hale, C. Leuschen, J. Paden, B. Pazer, E. Arnold, W. Blake, F. Rodriguez-Morales, J. Ledford *et al.*, "Antarctic ice depth-sounding radar instrumentation for the nasa dc-8," *IEEE Aerospace and Electronic Systems Magazine*, vol. 27, no. 3, pp. 4–20, 2012.
- [3] C. Leuschen, "Icebridge snow radar 11b geolocated radar echo strength profiles," *Boulder, Colorado USA: NASA DAAC at the National Snow and Ice Data Center*, 2010.
- [4] S. Gogineni, J.-B. Yan, J. Paden, C. Leuschen, J. Li, F. Rodriguez-Morales, D. Braaten, K. Purdon, Z. Wang, W. Liu *et al.*, "Bed topography of jakobshavn isbræ, greenland, and byrd glacier, antarctica," *Journal of Glaciology*, vol. 60, no. 223, pp. 813–833, 2014.
- [5] P. Perona and J. Malik, "Scale-space and edge detection using anisotropic diffusion," *IEEE Transactions on pattern analysis and machine intelligence*, vol. 12, no. 7, pp. 629–639, 1990.

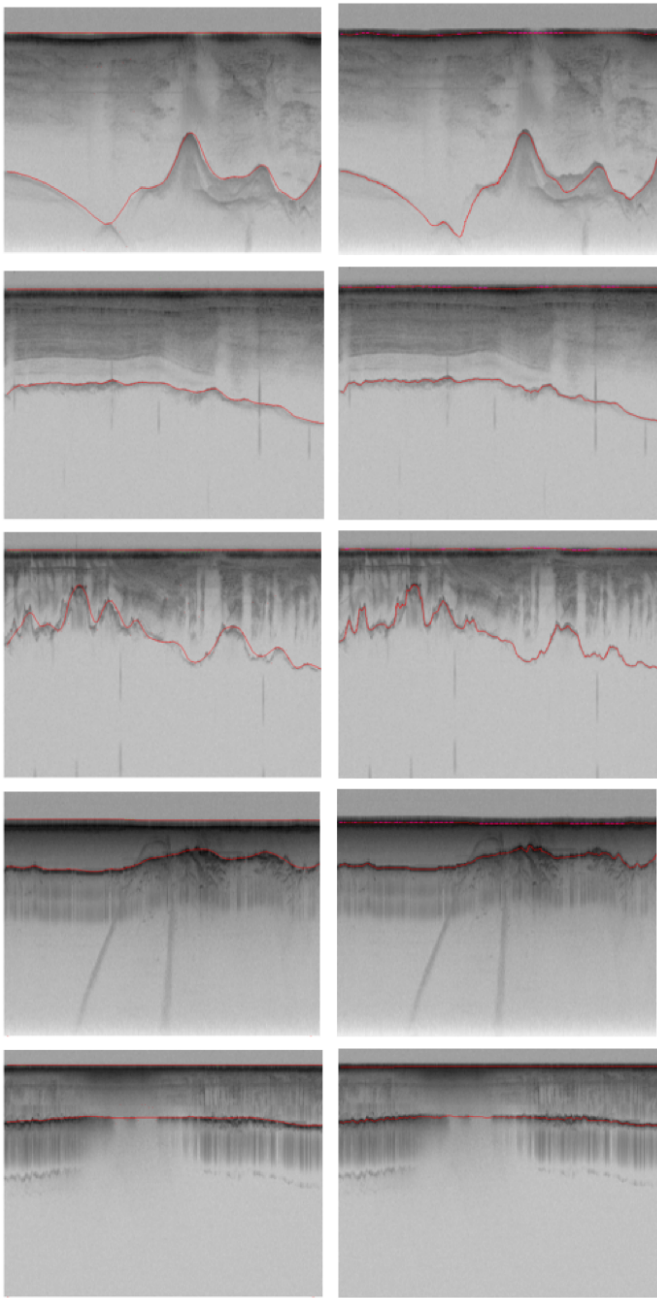


Fig. 8. Left column: our results in a diverse dataset which includes images with clutter, large variability of ice bottoms shape, surface multiples, and partially invisible ice bottoms, Right column: Ground-truth (manually labeled by human)

- [6] D. J. Crandall, G. C. Fox, and J. D. Paden, "Layer-finding in radar echograms using probabilistic graphical models," in *Pattern Recognition (ICPR), 2012 21st International Conference on*. IEEE, 2012, pp. 1530–1533.
- [7] M. Fahnestock, W. Abdalati, S. Luo, and S. Gogineni, "Internal layer tracing and age-depth accumulation relationships for the northern greenland ice sheet," *Journal of Geophysical Research*, vol. 106, no. D24, pp. 33 789–33 797, 2001.
- [8] A. Ferro and L. Bruzzone, "A novel approach to the automatic detection of subsurface features in planetary radar sounder signals," in *Geoscience and Remote Sensing Symposium (IGARSS), 2011 IEEE International*. IEEE, Conference Proceedings, pp. 1071–1074.
- [9] G. J. Freeman, A. C. Bovik, and J. W. Holt, "Automated detection of near surface martian ice layers in orbital radar data," in *Image Analysis*

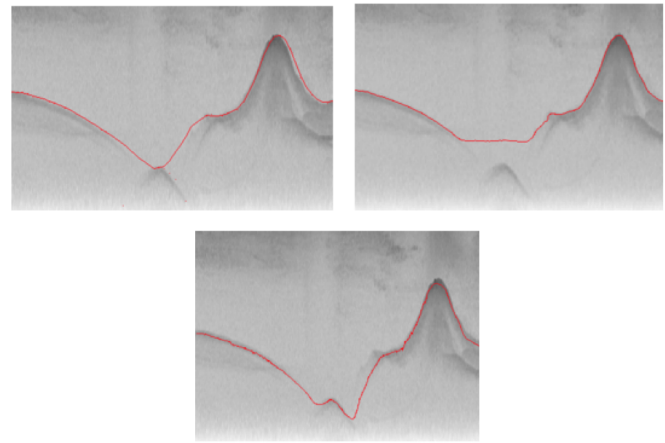


Fig. 9. The magnified image of the ice bottom of the first row of Figure 8. Top-Left: Our result, Top-right: State-of-the art method [22], Bottom: Ground-truth result

- & Interpretation (SSIAI), 2010 IEEE Southwest Symposium on. IEEE, Conference Proceedings, pp. 117–120.
- [10] H. Frigui, K. Ho, and P. Gader, "Real-time landmine detection with ground-penetrating radar using discriminative and adaptive hidden markov models," *EURASIP Journal on Advances in Signal Processing*, vol. 2005, no. 12, pp. 1867–1885, 2005.
- [11] C. M. Gifford, G. Finyom, M. Jefferson Jr, M. Reid, E. L. Akers, and A. Agah, "Automated polar ice thickness estimation from radar imagery," *Image Processing, IEEE Transactions on*, vol. 19, no. 9, pp. 2456–2469, 2010.
- [12] A.-M. Ilisei, A. Ferro, and L. Bruzzone, "A technique for the automatic estimation of ice thickness and bedrock properties from radar sounder data acquired at antarctica," in *Geoscience and Remote Sensing Symposium (IGARSS), 2012 IEEE International*. IEEE, Conference Proceedings, pp. 4457–4460.
- [13] N. B. Karlsson, D. Dahl-Jensen, S. P. Gogineni, and J. D. Paden, "Tracing the depth of the holocene ice in north greenland from radio-echo sounding data," *Annals of Glaciology*, vol. 54, no. 64, pp. 44–50, 2013.
- [14] S. Lee, J. Mitchell, D. J. Crandall, and G. C. Fox, "Estimating bedrock and surface layer boundaries and confidence intervals in ice sheet radar imagery using mcmc," in *Image Processing (ICIP), 2014 IEEE International Conference on*. IEEE, 2014, pp. 111–115.
- [15] J. E. Mitchell, D. J. Crandall, G. C. Fox, M. Rahneemofar, and J. D. Paden, "A semi-automatic approach for estimating bedrock and surface layers from multichannel coherent radar depth sounder imagery," in *SPIE Remote Sensing*. International Society for Optics and Photonics, Conference Proceedings, pp. 88 921–88 926.
- [16] J. E. Mitchell, D. J. Crandall, G. Fox, and J. Paden, "A semi-automatic approach for estimating near surface internal layers from snow radar imagery," in *IGARSS, Conference Proceedings*, pp. 4110–4113.
- [17] L. C. Sime, R. C. Hindmarsh, and H. Corr, "Instruments and methods automated processing to derive dip angles of englacial radar reflectors in ice sheets," *Journal of Glaciology*, vol. 57, no. 202, pp. 260–266, 2011.
- [18] C. Panton, "Automated mapping of local layer slope and tracing of internal layers in radio echograms," *Annals of Glaciology*, vol. 55, no. 67, pp. 71–77, 2014.
- [19] B. Smock and J. Wilson, "Reciprocal pointer chains for identifying layer boundaries in ground-penetrating radar data," pp. 602–605, 2012.
- [20] —, "Efficient multiple layer boundary detection in ground-penetrating radar data using an extended viterbi algorithm," pp. 83 571X–83 571X, 2012.
- [21] M. Rahneemofar, M. Yari, and G. C. Fox, "Automatic polar ice thickness estimation from sar imagery," in *SPIE Defense+ Security*. International Society for Optics and Photonics, 2016, pp. 982 902–982 902.
- [22] M. Rahneemofar, G. C. Fox, M. Yari, and J. Paden, "Automatic ice surface and bottom boundaries estimation in radar imagery based on level-set approach," *IEEE Transactions on Geoscience and Remote Sensing*, 2017.

- [23] M. Rahneemofar, A. Abbassi, and F. G. C. Paden, John, "Automatic ice thickness estimation in radar imagery based on charged particle concept," *IEEE International Geoscience and Remote Sensing Symposium*, 2017.
- [24] L. G. Roberts, "Machine perception of three-dimensional soups," Thesis, 1963.
- [25] J. M. Prewitt, "Object enhancement and extraction," *Picture processing and Psychopictorics*, vol. 10, no. 1, pp. 15–19, 1970.
- [26] D. Marr and E. Hildreth, "Theory of edge detection," *Proceedings of the Royal Society of London. Series B. Biological Sciences*, vol. 207, no. 1167, pp. 187–217, 1980.
- [27] J. Canny, "A computational approach to edge detection," *Pattern Analysis and Machine Intelligence, IEEE Transactions on*, no. 6, pp. 679–698, 1986.
- [28] J. S. Huang and D. H. Tseng, "Statistical theory of edge detection," *Computer vision, graphics, and image processing*, vol. 43, no. 3, pp. 337–346, 1988.
- [29] D. H. Lim and S. J. Jang, "Comparison of twosample tests for edge detection in noisy images," *Journal of the Royal Statistical Society: Series D (The Statistician)*, vol. 51, no. 1, pp. 21–30, 2002.
- [30] J. Lee, R. M. Haralick, and L. G. Shapiro, "Morphologic edge detection," *Robotics and Automation, IEEE Journal of*, vol. 3, no. 2, pp. 142–156, 1987.
- [31] J.-F. Rivest, P. Soille, and S. Beucher, "Morphological gradients," *Journal of Electronic Imaging*, vol. 2, no. 4, pp. 326–336, 1993.
- [32] T. S. Meese, R. J. Summers, D. J. Holmes, and S. A. Wallis, "Contextual modulation involves suppression and facilitation from the center and the surround," *Journal of Vision*, vol. 7, no. 4, p. 7, 2007.
- [33] M. Kass, A. Witkin, and D. Terzopoulos, "Snakes: Active contour models," *International journal of computer vision*, vol. 1, no. 4, pp. 321–331, 1988.
- [34] V. Caselles, R. Kimmel, and G. Sapiro, "Geodesic active contours," *International journal of computer vision*, vol. 22, no. 1, pp. 61–79, 1997.
- [35] G. Sundaramoorthi and A. Yezzi, "Global regularizing flows with topology preservation for active contours and polygons," *Image Processing, IEEE Transactions on*, vol. 16, no. 3, pp. 803–812, 2007.
- [36] X. Han, C. Xu, and J. L. Prince, "A topology preserving level set method for geometric deformable models," *Pattern Analysis and Machine Intelligence, IEEE Transactions on*, vol. 25, no. 6, pp. 755–768, 2003.
- [37] S. Lu, Z. Wang, and J. Shen, "Neuro-fuzzy synergism to the intelligent system for edge detection and enhancement," *Pattern Recognition*, vol. 36, no. 10, pp. 2395–2409, 2003.
- [38] P. J. Toivanen, J. Ansamki, J. Parkkinen, and J. Mielikinen, "Edge detection in multispectral images using the self-organizing map," *Pattern Recognition Letters*, vol. 24, no. 16, pp. 2987–2994, 2003.
- [39] H. Bustince, E. Barrenechea, M. Pagola, and J. Fernandez, "Interval-valued fuzzy sets constructed from matrices: Application to edge detection," *Fuzzy Sets and Systems*, vol. 160, no. 13, pp. 1819–1840, 2009.
- [40] D.-S. Kim, W.-H. Lee, and I.-S. Kweon, "Automatic edge detection using 3 3 ideal binary pixel patterns and fuzzy-based edge thresholding," *Pattern Recognition Letters*, vol. 25, no. 1, pp. 101–106, 2004.
- [41] F. Russo and G. Ramponi, "Edge extraction by fire operators," in *Fuzzy Systems, 1994. IEEE World Congress on Computational Intelligence., Proceedings of the Third IEEE Conference on*. IEEE, Conference Proceedings, pp. 249–253.
- [42] G. Sun, Q. Liu, Q. Liu, C. Ji, and X. Li, "A novel approach for edge detection based on the theory of universal gravity," *Pattern Recognition*, vol. 40, no. 10, pp. 2766–2775, 2007.
- [43] C. Lopez-Molina, H. Bustince, J. Fernandez, P. Couto, and B. De Baets, "A gravitational approach to edge detection based on triangular norms," *Pattern Recognition*, vol. 43, no. 11, pp. 3730–3741, 2010.
- [44] P. Dollar, Z. Tu, and S. Belongie, "Supervised learning of edges and object boundaries," in *Computer Vision and Pattern Recognition, 2006 IEEE Computer Society Conference on*, vol. 2. IEEE, Conference Proceedings, pp. 1964–1971.
- [45] P. Arbelaez, M. Maire, C. Fowlkes, and J. Malik, "Contour detection and hierarchical image segmentation," *Pattern Analysis and Machine Intelligence, IEEE Transactions on*, vol. 33, no. 5, pp. 898–916, 2011.
- [46] X. Ren, *Multi-scale improves boundary detection in natural images*. Springer, 2008, pp. 533–545.
- [47] C. A. de Coulomb, *Mmoires sur l'lectricit et le magntisme: extraits des Mmoires de l'acadmie royale des sciences de Paris, publis dans les annes 1785-1789*, 1806.